Int. J. Adv. Appl. Math. and Mech. 12(3) (2025) pages 99–109 (ISSN: 2347-2529)

Journal homepage: www.ijaamm.com

International Journal of Advances in Applied Mathematics and Mechanics

Application of the $\beta-$Rusanov scheme to two-dimensional shallow water equations and numerical simulation of a flooding phenomenon in a city

Research Article

Maman Yarodji Abdoul Kader[1]*, Badé Rabé[2], Yahaya Alassane Mahaman Nouri[3], Saley Bisso[2]

[1] *Department of Didactics of Disciplines, Djibo Hamani University, Tahoua, NIGER*

[2] *Department of Mathematics and Computer Science, Abdou Moumouni University, Niamey, NIGER*

[3] *National School of Engineering and Energy Sciences, University of Agadez, NIGER*

Volume 12, Issue 03

Received: 09 January 2025

Accepted (in revised version): 02 February 2025

Abstract: In this paper, the numerical resolution of the Saint-Venant system and the application to flooding phenomena were made. The system being conservative and hyperbolic, we used the finite volume method for the numerical resolution and the $\beta-$Rusanov scheme for the approximate the interfacial fluxes. We also present a numerical simulation of a flooding phenomenon in a residential area.

MSC: 35L65 • 37E35 • 76B07 • 76M12

Keywords: Finite volume method • Shallow water equations • Flooding phenomenon • $\beta-$Rusanov scheme

1. Introduction

A flood can be defined as an irruption of water on a normally dry ground or submersion by water overflowing its bed, or as an accumulation of water from drainages, in areas which are not normally submerged [1].
Globally many people live under threat floods. They are at the heart of the risk of disasters to which confronted the world. In Niger, these floods rank second among natural disasters after drought. For example, on September 8, 2020, the Niger River reached the highest level since the creation of the Niamey measuring station in 1929, i.e. 699 cm in height (source: Local Early Warning System for the Sirba floods (LEWSSF)). In a district of the capital of Niger named Lamordé, the dike gave way and various neighborhoods on the right bank, located in the lowest areas, were the first to suffer the throes of this scourge. Also, the heavy rain recorded (heights varying from 144.8 mm to 71.2 mm) in Niamey the capital city of Niger, on the night of August 10 to 11, 2021 caused the death of 5 people, according to the General Directorate of Civil Protection (GDCP). In addition, according to estimates from the Ministry of Humanitarian Action and Disaster Management as of September 23, 2021, 206457 people were affected by floods spread across 25888 households and 14884 collapsed houses. The same source highlights a considerable loss of livestock, the collapse of clute

* Corresponding author.
E-mail address(es): yalokmaman@gmail.com (Maman Yarodji Abdoul Kader), baderabe@yahoo.fr (Badé Rabé), alassane-nouri@yahoo.fr (Yahaya Alassane Mahaman Nouri), bsaley@yahoo.fr (Saley Bisso).

places, classrooms, wells, road infrastructure as well as thousands of hectares of buried crops. The report also shows 70 people died in these bad weather nationwide. The following year (2022), again according to GDCP, as of October 4, 2022, a total of 263671 people were affected by floods distributed in 32135 households. There was also a loss of 686 head of livestock, 89 classrooms and health huts and 14.5 tonnes of food destroying away by the water. On this date, the report also shows 192 people died in these bad weather nationwide. According to the latest data, dated September 04, 2024, from the Directorate of Preparedness, Warning and Disaster Management, the floods caused the collapse of more than 73,500 houses, affected more than 710,000 people, and caused the death of 273 people, including 121 by drowning and 152 by collapse. In addition to the loss of human life, infrastructure was not spared. Over 2,757 huts, 6,208 walls, 120 classrooms and 858 sheds were destroyed. Losses also included 1,920 granaries, 823 stores and 21,145 tonnes of foodstuffs, severely affecting the livelihoods of the inhabitants. In terms of livestock, almost 18,000 head perished, worsening an already critical situation for livestock-dependent communities.
To alleviate these problems, improving forecasting and prevention remains an essential tool of States, hence the need for the intervention of mathematicians.
In fluid dynamics, there is a system of partial differential equations (PDE), called the Saint-Venant system or the shallow water equations, which describes the flows of a fluid at a free surface.
Nowadays, it is widely used to describe many physical phenomena such as: runoff, oceanography, environmental protection, environmental pollution, climate change, dam break, sedimentology, flooding, etc... [2–5].

Barré of Saint-Venant obtained this non-linear system by vertical integration of the three-dimensional Navier-Stokes equations by formulating a certain number of hypotheses and physical approximations.
Despite its very wide use, the Saint-Venant system admits two major difficulties: on the one hand, taking into account the topography, and friction makes the numerical resolution complex; on the other hand the non-existence of an analytical solution. To remedy these difficulties, we approach the solution using a numerical methods. One of the methods generally used to approximate the solution of the Saint-Venant system is the finite volume method [6]. The interest of this method lies in the fact that it ensures the continuity of the mass which is the important property to respect in all calculations of fluid flows. The essential point of this numerical method being in the calculation of interfacial fluxes. Several numerical schemes have been developed to be able to calculate these fluxes. In this work, we will apply the $\beta-$Rusanov scheme to approach our numerical flux [7].

The paper is organised as follows. In section 2, we will present the two-dimensional shallow water equations with the terms of topography and friction, and its numerical resolution using the finite volume method. We use the hydrostatic reconstruction method with the well-balanced scheme and the apparent topography method to numerically process the source terms.
Section 3 is consecrated a test case on dam break on a domain with non-flat topography with three obstacles. We end the section with the numerical simulation of a flooding phenomenon in a residential area following a dam break with extremely important physical characteristics.

2. Numerical resolution of the shallow water equations

2.1. Two-dimensional shallow water equations with topography and friction terms

The derivative of the Navier-Stokes equations, under certain simplifying assumptions, namely the two-dimensional Saint-Venant system with source term, is given by:

$$\begin{cases} \dfrac{\partial h}{\partial t}+\dfrac{\partial hu}{\partial x}+\dfrac{\partial hv}{\partial y}=0 \\ \dfrac{\partial hu}{\partial t}+\dfrac{\partial}{\partial x}\left(hu^2+\dfrac{gh^2}{2}\right)+\dfrac{\partial huv}{\partial y}=-gh\left(\dfrac{\partial z}{\partial x}+S_{f_x}\right) \\ \dfrac{\partial hv}{\partial t}+\dfrac{\partial huv}{\partial x}+\dfrac{\partial}{\partial y}\left(hv^2+\dfrac{gh^2}{2}\right)=-gh\left(\dfrac{\partial z}{\partial y}+S_{f_y}\right), \end{cases} \tag{1}$$

where

- x and y are the horizontal spatial coordinates and t is time;
- $h(x,y,t)$ is the water depth at point (x,y) at time t;
- $u(x,y,t)$ et $v(x,y,t)$ are respectively the first and second components of the velocity vector at the point (x,y) at time t;
- g is the constant gravitational acceleration;
- $z(x,y)$ is the topography at point (x,y);

- $S_{f_x} = n^2 \frac{u\sqrt{u^2+v^2}}{h^{\frac{4}{3}}}$ et $S_{f_y} = n^2 \frac{v\sqrt{u^2+v^2}}{h^{\frac{4}{3}}}$ are respectively the term friction in the x and y directions with $n = \frac{1}{K_s}$ is the Manning's roughness coefficient and K_s is the Strickler coefficient.

The conservative form of the system eq. (1) is given by:

$$\frac{\partial U}{\partial t} + \frac{\partial \mathbf{f}(U)}{\partial x} + \frac{\partial \mathbf{g}(U)}{\partial y} = S(U), \tag{2}$$

with

$$U = \begin{pmatrix} h \\ hu \\ hv \end{pmatrix}; \; S(U) = \begin{pmatrix} 0 \\ S_{T_x} - ghS_{f_x} \\ S_{T_y} - ghS_{f_y} \end{pmatrix}; \; S_{T_x} = -gh\frac{\partial z}{\partial x}; \; S_{T_y} = -gh\frac{\partial z}{\partial y};$$

$$\mathbf{f}(U) = \begin{pmatrix} hu \\ hu^2 + \frac{1}{2}gh^2 \\ huv \end{pmatrix}; \tag{3}$$

$$\mathbf{g}(U) = \begin{pmatrix} hv \\ huv \\ hv^2 + \frac{1}{2}gh^2 \end{pmatrix}. \tag{4}$$

The jacobians matrix of fluxes eqs. (3) and (4) are respectively:

$$\frac{\partial \mathbf{f}}{\partial U} = \begin{pmatrix} 0 & 1 & 0 \\ gh - u^2 & 2u & 0 \\ -uv & v & u \end{pmatrix} \text{ and } \frac{\partial \mathbf{g}}{\partial U} = \begin{pmatrix} 0 & 0 & 1 \\ -uv & v & u \\ gh - v^2 & 0 & 2v \end{pmatrix}.$$

The associated eigenvalues are:

$$\begin{cases} \lambda_1\left(\frac{\partial \mathbf{f}}{\partial U}\right) = u + \sqrt{gh} \\ \lambda_2\left(\frac{\partial \mathbf{f}}{\partial U}\right) = u \\ \lambda_3\left(\frac{\partial \mathbf{f}}{\partial U}\right) = u - \sqrt{gh}. \end{cases} \text{ and } \begin{cases} \lambda_1\left(\frac{\partial g}{\partial U}\right) = v + \sqrt{gh} \\ \lambda_2\left(\frac{\partial \mathbf{g}}{\partial U}\right) = v \\ \lambda_3\left(\frac{\partial \mathbf{g}}{\partial U}\right) = v - \sqrt{gh}. \end{cases}$$

2.2. Apparent topography method

This method does not require a physical hypothesis [9, 10], but the main idea is to interpret the system eq. (1) as the shallow water equations with a new topography term $w = z + b$ where

$$\nabla b = S_f. \tag{5}$$

Thus, system eq. (1) is rewritten

$$\begin{cases} \frac{\partial h}{\partial t} + \frac{\partial hu}{\partial x} + \frac{\partial hv}{\partial y} = 0 \\ \frac{\partial hu}{\partial t} + \frac{\partial}{\partial x}\left(hu^2 + \frac{gh^2}{2}\right) + \frac{\partial huv}{\partial y} = -gh\frac{\partial w}{\partial x} \\ \frac{\partial hv}{\partial t} + \frac{\partial huv}{\partial x} + \frac{\partial}{\partial y}\left(hv^2 + \frac{gh^2}{2}\right) = -gh\frac{\partial w}{\partial y}. \end{cases} \tag{6}$$

2.3. Finite volume method

The numerical discretization of the eq. (1) is done by using the finite volume method [8], so let us consider a finite volume mesh: with mean a union of disjoint cells

$$\forall (i,j) \in \mathbb{Z}^2,\ C_{ij} = [x_{i-\frac{1}{2}}; x_{i+\frac{1}{2}}] \times [y_{j-\frac{1}{2}}; y_{j+\frac{1}{2}}], \tag{7}$$

centered at $x_i = \dfrac{x_{i-\frac{1}{2}} + x_{i+\frac{1}{2}}}{2}$ and $y_j = \dfrac{y_{j-\frac{1}{2}} + y_{j+\frac{1}{2}}}{2}$, where the discrete points in space $(x_{i+\frac{1}{2}})_{i\in\mathbb{Z}}$ and $(y_{j+\frac{1}{2}})_{j\in\mathbb{Z}}$ are defined respectively

$$x_{i+\frac{1}{2}} = \left(i + \frac{1}{2}\right)\Delta x \ \text{ and } \ y_{j+\frac{1}{2}} = \left(j + \frac{1}{2}\right)\Delta y.$$

Let us denote Δt the time step and U_{ij}^n the approximation of the cell average of the exact solution $u(x,y,t)$ at time $t^n = n\Delta t$. The finite volume method consists to integrate the system on $[t^n, t^{n+1}] \times C_{ij}$, which gives:

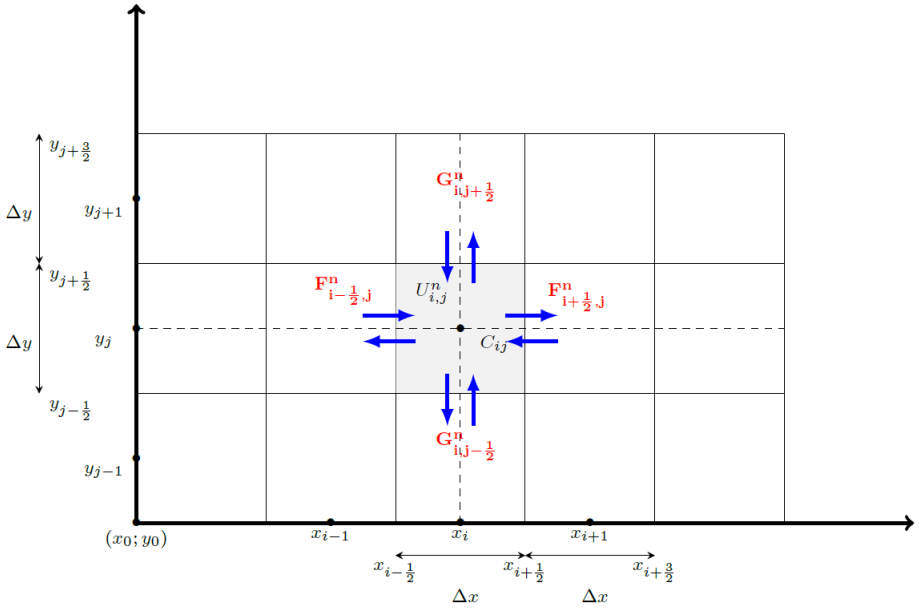

Fig. 1. Rectangular mesh of the 2D domain

$$U_{i,j}^{n+1} = U_{i,j}^n - \frac{\Delta t}{\Delta x}\left(F^n_{i+\frac{1}{2}G,j} - F^n_{i-\frac{1}{2}D,j}\right) - \frac{\Delta t}{\Delta y}\left(G^n_{i,j+\frac{1}{2}G} - G^n_{i,j-\frac{1}{2}D}\right), \tag{8}$$

with

$$F^n_{i\pm\frac{1}{2}G,j} = \mathscr{F}\left(U^n_{i\pm\frac{1}{2}G,j}, U^n_{i\pm\frac{1}{2}D,j}, \Delta z_{i\pm\frac{1}{2},j} + \Delta b^n_{i\pm\frac{1}{2},j}\right);$$

$$G^n_{i,j\pm\frac{1}{2}G} = \mathscr{G}\left(U^n_{i,j\pm\frac{1}{2}G}, U^n_{i,j\pm\frac{1}{2}D}, \Delta z_{i,j\pm\frac{1}{2}} + \Delta b^n_{i,j\pm\frac{1}{2}}\right);$$

where $\Delta z_{i\pm\frac{1}{2},j} = z_{i\pm1,j} - z_{i,j}$ and $\Delta z_{i,j\pm\frac{1}{2}} = z_{i,j\pm1} - z_{i,j}$ are the topography at the interface. To obtain $\Delta b^n_{i\pm\frac{1}{2},j}$ and $\Delta b^n_{i,j\pm\frac{1}{2}}$, we explicitly discretize eq. (5) on $[t^n, t^{n+1}] \times C_{i,j}$. Which gives us:

$$\begin{cases} \Delta b^n_{i\pm\frac{1}{2},j} = \Delta x S^n_{f_{x_{i\pm\frac{1}{2},j}}} \\ \\ \Delta b^n_{i,j\pm\frac{1}{2}} = \Delta y S^n_{f_{y_{i,j\pm\frac{1}{2}}}} \end{cases}.$$

Using Manning's formula, we have:

$$S^n_{f_{x_{i\pm\frac{1}{2},j}}} = \begin{cases} 0, \quad \text{if } h^n_{i,j} = h^n_{i\pm1,j} = 0 \\ \\ n^2 \dfrac{u^n_{i\pm\frac{1}{2},j}\sqrt{{u^n_{i\pm\frac{1}{2},j}}^2 + {v^n_{i,j}}^2}}{{h^n_{i\pm\frac{1}{2},j}}^{\frac{4}{3}}}, \quad \text{otherwise.} \end{cases} \tag{9}$$

$$S^n_{f_{y_{i,j\pm\frac{1}{2}}}} = \begin{cases} 0, \quad \text{if } h^n_{i,j} = h^n_{i,j\pm1} = 0 \\ n^2 \dfrac{v^n_{i,j\pm\frac{1}{2}} \sqrt{{u^n_{i,j}}^2 + {v^n_{i,j\pm\frac{1}{2}}}^2}}{{h^n_{i,j\pm\frac{1}{2}}}^{\frac{4}{3}}}, \quad \text{otherwise.} \end{cases} \tag{10}$$

2.4. Flux approximation

We use the new variant of Rusanov scheme, to know the $\beta-$Rusanov scheme [7]. Let us note U^*_L and U^*_R the data in the two neighboring cells, then the $\beta-$Rusanov flux is gives by:

$$\mathscr{F}(U^*_L, U^*_R) = \frac{\mathbf{f}(U^*_L) + \mathbf{f}(U^*_R)}{2} - \kappa \frac{U^*_R - U^*_L}{2}; \tag{11}$$

where κ is the maximum wave velocity by calculating the maximum eigenvalue of the local Jacobian matrix of the cell and the new reconstructed data are obtained by:

$$U^*_R = U_R - \frac{\beta}{2}(U_R - U_L) \text{ and } U^*_L = U_L + \frac{\beta}{2}(U_R - U_L);$$

with β a real such as $|\beta| < 1$.

The time step discretization Δt is chosen such that the following condition:

$$\Delta t = \varepsilon \frac{\min(\Delta x, \Delta y)}{\kappa(1-\beta)};$$

be satisfied, $\kappa = \max(|\lambda_k|_{k\in\{1;2;3\}})$ and $\varepsilon \in]0;1[$.

2.5. Traitement of the bottom topography

We use the well-balanced method which consists to decenter the source term, S_T, at the interfaces and based on the hydrostatic reconstruction method [8, 11, 12]. The latter method is based on the idea that near the equilibrium, the flows are almost hydrostatic.

The reconstructed states are defined by:

$$h_{i+\frac{1}{2}L,j} = \max\left(0; h_{i,r,j} - \max(0, \Delta z_{i+\frac{1}{2},j})\right); \quad h_{i+\frac{1}{2}R,j} = \max\left(0; h_{i+1,\ell,j} + \max(0, \Delta z_{i+\frac{1}{2},j})\right);$$

$$h_{i,j+\frac{1}{2}L} = \max\left(0; h_{i,j,r} - \max(0, \Delta z_{i,j+\frac{1}{2}})\right); \quad h_{i,j+\frac{1}{2}R} = \max\left(0; h_{i,j+1,\ell} + \max(0, \Delta z_{i,j+\frac{1}{2}})\right).$$

Using the reconstructed values, we have:

$$S^n_{T_{x_{i+\frac{1}{2}L,j}}} = \begin{pmatrix} 0 \\ g\dfrac{h^2_{i+\frac{1}{2}L,j} - h^2_{i,r,j}}{2} \\ 0 \end{pmatrix}; \quad S^n_{T_{x_{i-\frac{1}{2}R,j}}} = \begin{pmatrix} 0 \\ g\dfrac{h^2_{i-\frac{1}{2}R,j} - h^2_{i,\ell,j}}{2} \\ 0 \end{pmatrix};$$

$$S^n_{T_{x_{i,j}}} = S^n_{T_{x_{i+\frac{1}{2}L,j}}} - S^n_{T_{x_{i-\frac{1}{2}R,j}}};$$

$$S^n_{T_{y_{i,j+\frac{1}{2}L}}} = \begin{pmatrix} 0 \\ 0 \\ g\dfrac{h^2_{i,j+\frac{1}{2}L} - h^2_{i,j,r}}{2} \end{pmatrix}; \quad S^n_{T_{y_{i;j-\frac{1}{2}R}}} = \begin{pmatrix} 0 \\ 0 \\ g\dfrac{h^2_{i,j-\frac{1}{2}R} - h^2_{i,j,\ell}}{2} \end{pmatrix};$$

$$S^n_{T_{y_{i,j}}} = S^n_{T_{y_{i,j+\frac{1}{2}L}}} - S^n_{T_{y_{i;j-\frac{1}{2}R}}}.$$

The reconstructed variables are given by:

$$U^n_{i+\frac{1}{2}L,j} = \begin{pmatrix} h^{*n}_{i+\frac{1}{2}L,j} \\ h^{*n}_{i+\frac{1}{2}L,j} u^*_{i,r,j} \\ h^{*n}_{i+\frac{1}{2}L,j} v^*_{i,r,j} \end{pmatrix}; \quad U^n_{i+\frac{1}{2}R,j} = \begin{pmatrix} h^{*n}_{i+\frac{1}{2}R,j} \\ h^{*n}_{i+\frac{1}{2}R,j} u^*_{i+1,\ell,j} \\ h^{*n}_{i+\frac{1}{2}R,j} v^*_{i,r,j} \end{pmatrix};$$

$$U^n_{i,j+\frac{1}{2}L} = \begin{pmatrix} h^{*n}_{i,j+\frac{1}{2}L} \\ h^{*n}_{i,j+\frac{1}{2}L} u^*_{i,j,r} \\ h^{*n}_{i,j+\frac{1}{2}L} v^*_{i,j,r} \end{pmatrix}; \quad U^n_{i,j+\frac{1}{2}R} = \begin{pmatrix} h^{*n}_{i,j+\frac{1}{2}R} \\ h^{*n}_{i,j+\frac{1}{2}R} u^*_{i,j,r} \\ h^{*n}_{i,j+\frac{1}{2}R} v^*_{i,j+1,\ell} \end{pmatrix}.$$

3. Numerical results

3.1. Dam break with three obstacles and with term friction

We consider a rectangular domain of dimension $[0;200] \times [0;150]$. Three obstacles are placed, two of which are pillars of 9 m in height and a hump of 5 m in height. Our objectives for this benchmark are to observe the behaviors of the water depth profiles and how the water will bypass the base of the hump.
The function describing the bottom topography is given by:

$$z(x,y) = \begin{cases} \dfrac{1}{250 + \max(|x|;|y|)}, & \text{if } (x,y) \in [50;90] \times [10;40] \\ \dfrac{1}{200 + \max(|x|;|y|)}, & \text{if } (x,y) \in [50;90] \times [95;120] \\ \dfrac{1}{500 + (x-120)^2 + (y-80)^2}, & \text{otherwise.} \end{cases} \tag{12}$$

Scale: $\begin{cases} 1 \to 0,045\ m, & \text{on the abscissa} \\ 1 \to 0,04\ m, & \text{in ordonate.} \end{cases}$ We have discretized the calculation domain into a grid of 8000 rectangles whose space steps are $\Delta x = 2$ and $\Delta y = 1,875$.
We assume that at time $t = 0$ s the dam collapses with a water flow $q(x,y,0) = 3.75\ m^3/\text{s}$ and $h(x,y,0) + z(x,y) = 5\ m$.
The Manning friction coefficient is equal to $n = 0.018$ and the chosen parameter is $\beta = -0.8$.

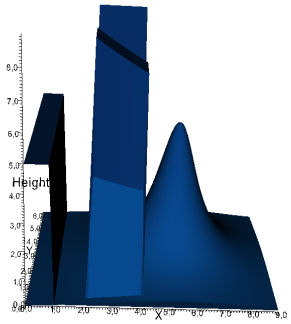

Fig. 2. Variation of the water depth at $t = 0$ s

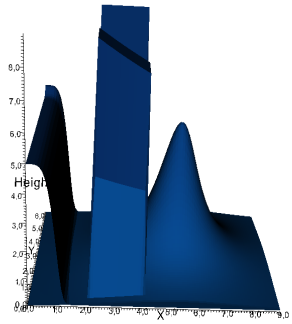

Fig. 3. Variation of the water depth at $t = 0,39$ s

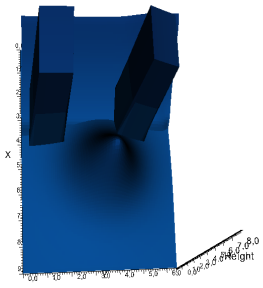

Fig. 4. Variation of the water depth at $t = 3,96$ s

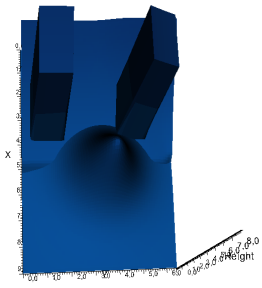

Fig. 5. Variation of the water depth at $t = 6,24$ s

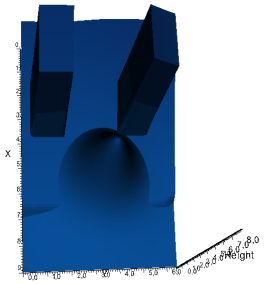

Fig. 6. Variation of the water depth at $t = 8,92$ s

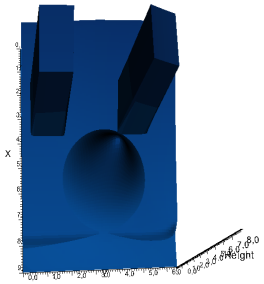

Fig. 7. Variation of the water depth at $t = 10,73$ s

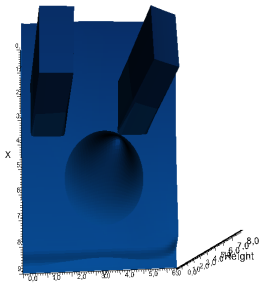

Fig. 8. Variation of the water depth at $t = 11,65$ s

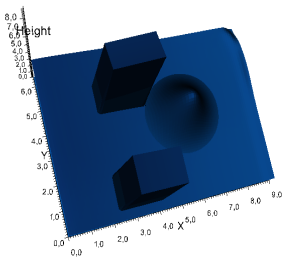

Fig. 9. Variation of the water depth at $t = 12,90$ s

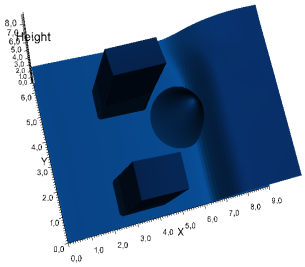

Fig. 10. Variation of the water depth at $t = 25,68$ s

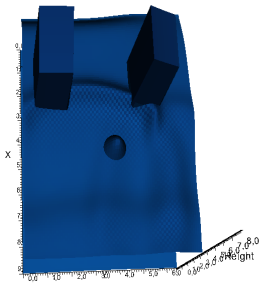

Fig. 11. Variation of the water depth at $t = 44,50$ s

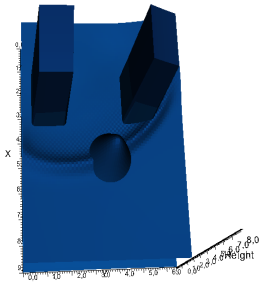

Fig. 12. Variation of the water depth at $t = 104,24$ s

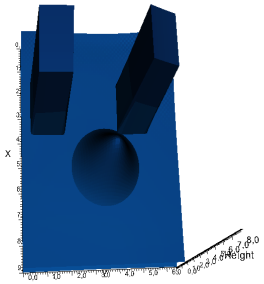

Fig. 13. Variation of the water depth at $t = 169$ s

Analysis of results

Figure 2 illustrates the topography of the land and the dam placed at the position $x = 20$ m over an area 200 m long and 150 m wide. Below the effect of gravity, we have a slight variation in the height of the water on fig. 3. Following the continuous arrival of water, we see in figs. 4 and 9, rising water and avoiding obstacles. We also observe, the water slightly encircles the bump and invades its entire base at time $t = 12,90$ s. With the solid boundary downstream, we notice in fig. 10 to fig. 12, the return of the height of the water and the hump submerged except for a small part of its crest. In addition, the water reaching upstream continues to hit obstacles and makes pitching to stabilize. We conclude that at time $t = 169$ s, the height of the water is in a state of equilibrium.

3.2. Numerical simulation of a flooding phenomenon in a virtual city

The objective of this simulation is to measure the risk of flooding in an environment urban located downstream of a dam 6 m high and 3000 m wide. We consider a rectangular terrain of dimension $[0;5000] \times [0;3000]$ having a topography defined by:

$$z(x,y) = \begin{cases} \dfrac{1}{2000+\max(|x|;|y|)}, & \text{if } (x,y) \in [600;1000] \times [2500;2900] \\ \dfrac{1}{4\sqrt{10\pi}} e^{-\frac{(x-1200)^2}{1600}} \times e^{-\frac{(y-2200)^2}{10000}}, & \text{if } (x,y) \in [1000;2000] \times [2000;2900] \\ \dfrac{1}{2000+\max(|x|;|y|)}, & \text{if } (x,y) \in [1000;1500] \times [100;500] \\ \dfrac{1}{2000+(y-1500)^2}, & \text{if } (x,y) \in [1000;1500] \times [600;2000] \\ \dfrac{1}{2000+\max(|x|;|y|)}, & \text{if } (x,y) \in [2500;3500] \times [2500;2900] \end{cases} \tag{13}$$

$$\begin{cases} \dfrac{1}{2000+\max(|x|;|y|)}, & \text{if } (x,y) \in [2500;3500] \times [200;700] \\ \dfrac{1}{2000+(x-2900)^2+(y-1500)^2}, & \text{if } (x,y) \in [2500;3500] \times [600;2000] \\ \dfrac{1}{2000+(x-4500)^2}, & \text{if } (x,y) \in [4000;4900] \times [1200;2000] \\ \dfrac{1}{2000+(x-4500)^2}, & \text{if } (x,y) \in [4000;4900] \times [200;700] \\ \dfrac{1}{2000+\max(|x|;|y|)}, & \text{if } (x,y) \in [4000;4900] \times [2300;2900]. \end{cases} \tag{14}$$

Scale: $\begin{cases} 1 \to 0,0022\ m, & \text{on the abscissa} \\ 1 \to 0,0026\ m, & \text{in ordonate.} \end{cases}$

In the initial state, the flow is assumed to be at rest with a water height given by $h(x, y, 0) = 6 - z(x, y)$ for $x < 300$ and $h(x, y, 0) = 0.05 - z(x, y)$ otherwise. The calculation domain is discretized into a grid of 8925 rectangles. The boundary conditions are of the solid boundary type. The time step Δt is chosen such that the following condition is satisfied:

$$\Delta t = \varepsilon \frac{\min(\Delta x, \Delta y)}{\max(|\lambda_i|_{i\in\{1;2;3\}})(1-\beta)}.$$

The coefficient of friction is equal to $n = 0,018$ et $\beta = -0,7$.

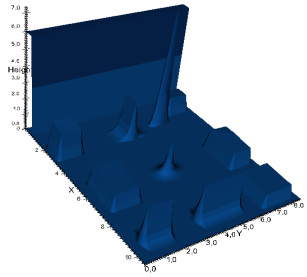

Fig. 14. Water depth profile at $t = 0$ s

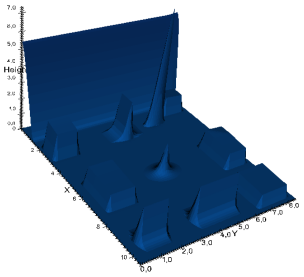

Fig. 15. Water depth profile at $t = 25,09$ s

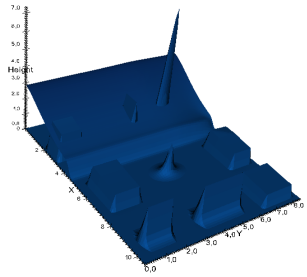

Fig. 16. Water depth profile at $t = 130,69$ s

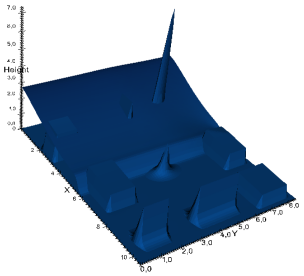

Fig. 17. Water depth profile at $t = 190,72$ s

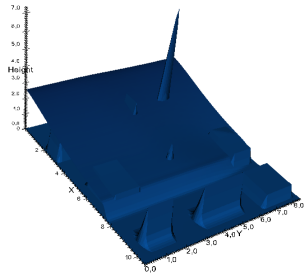

Fig. 18. Water depth profile at $t = 238,82$ s

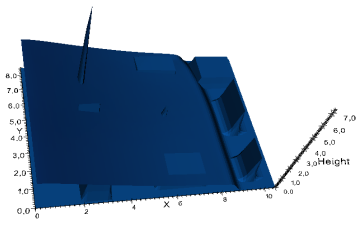

Fig. 19. Water depth profile at $t = 281,07$ s

Analysis of results

Figure 14 illustrates the level of the dam before its collapse, the morphology of the ground and the residential area. The latter is made up of residential houses represented by the parallelepipeds, a residential building, two-story houses

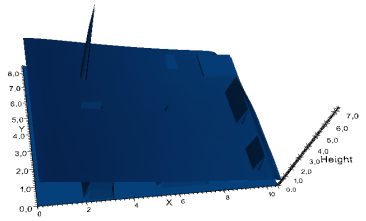

Fig. 20. Water depth profile at $t = 353,50$ s

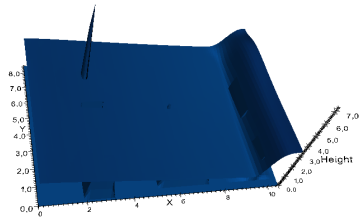

Fig. 21. Water depth profile at $t = 497$ s

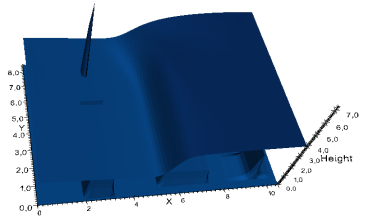

Fig. 22. Water depth profile at $t = 904,37$ s

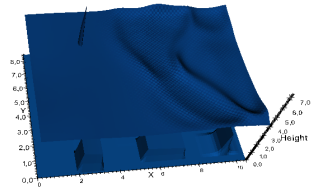

Fig. 23. Water depth profile at $t = 1392,75$ s

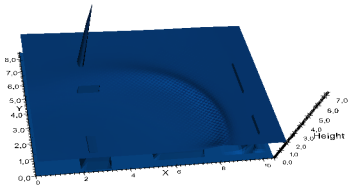

Fig. 24. Water depth profile at $t = 5936,14$ s

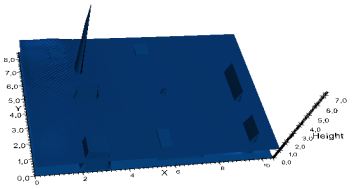

Fig. 25. Water depth profile at $t = 9180$ s

and a roundabout in the middle. Under the effect of gravity, in the figures from fig. 15 to fig. 16, we see the beginning of the dam break and the submersion of the constructions by water. The figures from fig. 17 to fig. 20 show the water conquering the entire neighborhood. In addition, we notice several houses are already underwater and for some, only the roof remains. Following the blockage downstream, in fig. 21 we have the beginning of the return of the water depth. We see in the figures from fig. 22 to fig. 24 all the houses are invaded and are under water of 4 m immersion except the building. In the same figures, we observe the roof of certain constructions after submersion and the wave propagation following the arrival and return of water. At the moment $t = 9180$ s, we notice that the scheme is in the equilibrium state, the whole neighborhood is flooded, the water is half the height of several of habitats and for some houses, we only see their roofs.

4. Conclusion

We have solved numerically, by the finite volume method, the two-dimensional shallow water equations with source term by treating the term friction by the apparent topography method. A dam break simulation on a non-flat bottom with obstacles was carried out to examine the capacity and precision of the $\beta-$Rusanov scheme to simulate free surface flow with a very large quantity of water and in a domain with complex geometry. In addition, the construction of a virtual residential neighborhood, using mathematical functions, was done in order to simulate a flooding phenomenon on real configurations following a dam break upstream of the city.
Therefore, we affirm the robustness, accuracy, speed and ability of the $\beta-$Rusanov scheme to reproduce or imitate physical phenomena with complex structure. It can be used in the construction of examples that will allow to understand many natural phenomena.

References

[1] Christophe Ancey, Hydraulique à surface libre, EPFL, ENAC/IIC/LHE, Ecublens, CH-1015 Lausanne, Suisse.

[2] F. Benkhaldoun, I. Elmahi and M. Seaid, Well-balanced finite volume schemes for pollutant transport on unstructured meshes, Journal of Computational Physics, 226(1)(2006) 180-203.

[3] V. Caleffi, A. Valiani and A. Zanni, Finite volume method for simulating extreme flood events in natural channels, Journal of Hydraulic Research. 41(2)(2003) 167-177.

[4] H. Derakhshan and M.Z. Bistkonj, A New Two Dimensional Model for Pollutant Transport in Ajichai River, Journal of Hydraulic Structures, 1(2)(2013) 44-54.

[5] G. Navarro, P. Fras, A. and I. Villanueva, Dam-break flow simulation : some results for one-dimensional models of real cases, Journal of Hydrology, 216(3-4)(1999) 227-247

[6] R.J. LeVeque, Finite Volume Methods for Hyperbolic Problems, Cambridge University Press, Cambridge, 2002.

[7] M. Y. A. Kader, R. Badé and B. Saley, A new variant of Rusanov scheme: $\beta-$Rusanov for numerical resolution of shallow water flows, Int. J. of Appl. Math., 35(4)(2022) 585-600

[8] M.Y.A. Kader, R. Badé and B. Saley. Study of the 1D Saint-Venant Equations and Application to the Simulation of a Flood Problem. Journal of Applied Mathematics and Physics, 8(2020) 1193-1206

[9] F. Bouchut, Nonlinear stability of finite volume methods for hyperbolic conservation laws, and well-balanced schemes for sources, Birkhäuser Verlag, P.O. Box 133, CH-4010 Basel, Switzerland, (2)2004.

[10] F. Bouchut and T. Morales, A subsonic-well-balanced reconstruction scheme for shallow water flows, SIAM Journal on Numerical Analysis, January 2010.

[11] E. Audusse, F. Bouchut, M. O. Bristeau, R. Klein and B. Perthame, A fast and stable well-balanced scheme with hydrostatic reconstruction for shallow water flows, SIAM Journal on Scientific Computing, 25(6)(2006) 2050-2065.

[12] A. Duran, Q. Liang and F. Marche, On the well-balanced numerical discretization of shallow water equations on instructured meshes, Journal of Computational Physics, 235(2013) 565-585.